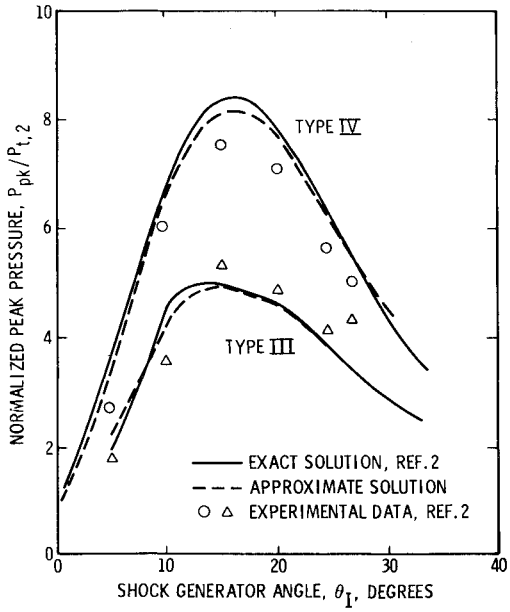

Fig. 3 Peak pressures for Type III and IV interference for $M_\infty = 6$, $\gamma = 1.4$.

number and pressure and the strength of the impinging shock are known. Basically, an iterative solution scheme using the Rankine-Hugoniot relations is utilized to determine the shear layer deflections aft of shock intersection points which result in equal pressures above and below the shear layers.

In the present Note, two approximations are introduced. First, the pressures behind the nearly normal shock waves at Points A and C are approximated by those behind normal shocks. This approximation is motivated by the fact that for Type III and IV interference the strong shock inclination does not differ greatly from a normal shock, and the pressure behind it is not a strong function of its inclination. This assumption eliminates the iterations on shear layer deflections required in the exact solution; in all other respects, however, the computation is identical to the exact solution.[2] A further simplification is possible if graphical solutions[6] or closed-form representations of the Rankine-Hugoniot relations[7,8] are utilized. The second approximation is the assumption that the transition from Type III to Type IV interference occurs when the flow bounded by Region ABC is unable to turn tangent to the body at Point B through an attached shock. It is further assumed that this detachment angle is given by the two-dimensional wedge value for the shear layer impingement on a two-dimensional body, and by the conical value for impingement on a three-dimensional body.

The results of the present theory are compared with the exact solution[2] and experimental data[2] for $M_\infty = 6$ in Figs. 1–3. The interference patterns were generated by impinging a planar shock on the bow shock of a 2-in. hemisphere, which was instrumented with pressure orifices. Details of the experimental apparatus are given in Ref. 2. The initial deflections of the shear layer and the transmitted shock are presented as a function of the strength of the impinging shock (expressed by the shock generator angle, θ_1) in Fig. 1. The experimental data were obtained from schlieren photographs, and the data points represent the mean values with the error bars indicating the maximum excursion from the mean. As may be seen, there is good agreement between the approximate and exact solutions and the experimental data.

Figure 2 presents results for the transition from Type III to IV for various strength impinging shock waves. The experimental data were determined by examining both schlieren photographs and pressure distributions. For a given strength impinging shock wave, if $\gamma_I > \gamma_D$, Type III interference results; otherwise Type IV occurs. With the exception of the point $\beta_I = 13°$, good agreement is obtained between the two theoretical predictions and the experimental data.

The final comparison is presented in Fig. 3, in which the normalized peak pressures for Types III and IV interference are plotted as a function of the impinging shock generator angle. For Type III the peak pressure is that associated with a sharp cone having a semi-vertex angle of $90 + \theta_F - \gamma_D$ in a freestream with a Mach number and static pressure equal to that computed for Region ABC. For Type IV the peak pressure is that associated with flow behind a normal shock in a freestream with a Mach number and static pressure equal to that computed for the supersonic jet. In both cases, the pressure is normalized by the freestream impact pressure. Again there is good agreement between the two theories and the experimental data.

In conclusion, a simple technique has been presented for calculating Types III and IV interference. The method has been shown to be in good agreement with the exact solution and experimental data for $M_\infty = 6$. This technique, when used in conjunction with empirical pressure-heat-transfer correlations,[2] thus provides a rapid estimate of the heat transfer associated with these two types of interference.

References

[1] Edney, B. E., "Anomalous Heat Transfer and Pressure Distributions on Blunt Bodies at Hypersonic Speeds in the Presence of an Impinging Shock," FFA Rept. 115, Feb. 1968, The Aeronautical Institute of Sweden, Stockholm, Sweden.

[2] Edney, B. E., Bramlette, T. T., Ives, J., Hains, F. D., and Keyes, J. W., "Theoretical and Experimental Studies of Shock Interference Heating," Rept. 9500-920-195, Oct. 1970, Bell Aerospace Co., Buffalo, N.Y.

[3] Hains, F. D. and Keyes, J. W., "Shock Interference Heating in Hypersonic Flows," *AIAA Journal*, Vol. 10, No. 11, Nov. 1972, pp. 1441–1447.

[4] Crawford, D. H., "A Graphical Method for the Investigation of Shock Interference Phenomena," *AIAA Journal*, Vol. 11, No. 11, Nov. 1973, pp. 1590–1592.

[5] Edney, B. E., private communication, Oct. 1970, Bell Aerospace Co., Buffalo, N.Y.

[6] "Equations, Tables, and Charts for Compressible Flow," Rept. 1135, 1953, NACA.

[7] Hill, W. G., "A Convenient, Explicit Formula for Oblique Shock Calculations," *Journal of Aircraft*, Vol. 5, No. 5, Sept.–Oct. 1968, pp. 509–510.

[8] Simon, W. E. and Walter, L. A., "Approximations for Supersonic Flow over Cones," *AIAA Journal*, Vol. 1, No. 7, July 1963, pp. 1696–1698.

Laminar Boundary Layer Behind a Shock Wave Propagating Along Perforated Walls

K. TAKAYAMA*
Tohoku University, Sendai, Japan

IN connection with studies on the motion of the shock wave in shock tubes, the laminar boundary layer behind the shock wave propagating along a duct of perforated walls is analyzed. Recently a few studies[1–3] have been known as to the shock-wave attenuation in a perforated duct. From the experimental evidence, it is found that the shock attenuation rates, which are practically

Received December 3, 1973; revision received February 12, 1974.
Index category: Boundary Layers and Convective Heat Transfer—Laminar.

* Lecturer, Institute of High Speed Mechanics.

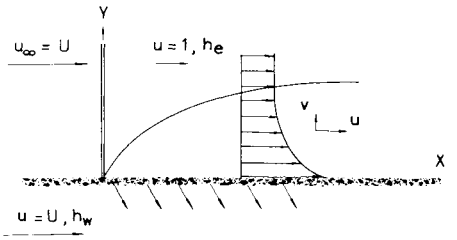

Fig. 1 Shock fixed coordinates. Subscripts e and w mean conditions in the main flow and at the wall.

of interest, and the curvatures of the incident shock wave are caused mainly by the wavelets in inviscid flow and existence of the boundary layer.

As the first step to investigate the problem, this Note is concerned with a boundary-layer suction problem in the compressible flow. For uniform and small perforation ratios, the shock-wave velocity can be assumed to be constant and then the pressure gradient can be also ignored as a first approximation. Therefore, the problem can be reduced to that of the flat plate boundary-layer flow with suction.

Figure 1 shows the flowfield in the shock-fixed coordinates.[4] Here the velocity and the specific enthalpy are nondimensionalized by the velocity in the main flow, u_e; that is, $u \to u/u_e$, and $h \to h/u_e^2$, and the coordinates are also expressed by the characteristic length L—for instance the diameter of the shock tube—$X, Y \to X, Y/L$ as shown in Fig. 1.

Introducing the boundary-layer coordinates[5]

$$\eta = (Re/2X)^{1/2} \int \frac{\rho}{\rho_e} dY, \quad \xi = \varepsilon(2XRe)^{1/2} \tag{1}$$

where $Re = u_e L \rho_e/\mu_e$ is the Reynolds number which refers to the conditions in the main flow, ρ_e the density in the main flow, and $\varepsilon \to -\rho_w v_w/\rho_e u_e$ the dimensionless mass flux through perforations for unit area, which will be thought to be constant for the shock Mach number $M_s \geqq 1.33$ and $\gamma = 1.4$, because the choking conditions are valid for mass flux through perforations.

Assuming $\rho\mu = \text{const}$ and Prandtl number $Pr = 0.7$ for air, basic equations are

$$\begin{aligned} f''' + ff'' &= \xi(f' f_\xi' - f_\xi f'') \\ g'' + Prfg' &= -E(f'')^2 + Pr\xi(f' g_\xi - f_\xi g') \end{aligned} \tag{2}$$

where E is a kind of Eckert number defined by $Pr/(h_e - h_w)$, $f' = u$, and $g = (h - h_w)/(h_e - h_w)$.

Boundary conditions are

$$\begin{aligned} &\eta \to 0, \quad f' = U, \quad f + \xi f_\xi = \xi, \quad g = 0 \\ &n \to \infty, \quad f' = 1, \quad g = 1 \end{aligned} \tag{3}$$

To seek the solutions of Eqs. (2) under the boundary conditions Eqs. (3), f and g can be expanded in terms of ξ for small perforation ratios; that is,

$$f = \sum_{n=0}^{\infty} \xi^n f_n, \quad g = \sum_{n=0}^{\infty} \xi^n g_n$$

Table 1 Velocity gradients at the wall

U	f_0''	f_1''	f_2''	f_3''	f_4''
0.0	0.4696	0.6083	0.1322	−0.0290	0.0046
2.0	−1.0191	−0.4785	−0.0739	−0.0008	0.0009
4.0	−4.0622	−1.3945	−0.1628	−0.0027	0.0010
6.0	−8.1006	−2.2973	−0.2233	−0.0036	0.0009

Table 2 Reduced enthalpy gradients at the wall

U	g_0'	g_1'	g_2'	g_3'	g_4'
0.0	0.4400	0.4764	0.0684	−0.0126	0.0024
2.0	1.0908	0.4322	0.0585	0.0010	−0.0005
4.0	1.6957	0.4919	0.0510	0.0011	−0.0002
6.0	2.1542	0.5147	0.0444	0.0009	−0.0001

Thus basic equations for ξ^n terms are

$$\begin{aligned} &f_n''' + \sum_{i=0}^{n} (i+1) f_i f_{n-i}'' = \sum_{i=0}^{n} (n-i) f_i' f_{n-i}' \\ &g_n'' + Pr \sum_{i=0}^{n} (i+1) f_i g_{n-i}' = \sum_{i=0}^{n} \{ -E f_i'' f_{n-i}'' + Pr(n-i) f_i' g_{n-i} \} \end{aligned} \tag{4}$$

The abovementioned equations and their boundary conditions for $n = 0$ terms coincide with ones given by Mirels[4] and the equations for other terms are immediately found to be linear. The boundary conditions are

$$\begin{aligned} &f_1(0) = 0.5, \quad f_1'(0) = f_1'(\infty) = g_1(0) = g_1(\infty) = 0, \text{ for } n = 1 \\ &f_n(0) = f_n'(0) = f_n'(\infty) = g_n(0) = g_n(\infty) = 0, \text{ for } n > 1 \end{aligned} \tag{5}$$

If the zeroth-order solutions are known, then the higher-order solutions can be successively determined by means of numerical integrations, such as Runge-Kutta-Gill's method. In Tables 1 and 2, the results are shown and, of course, the velocity gradient functions for $n = 0$ are the same as Mirels' results.

At far behind the shock wave, the asymptotic suction profile will be obtained such as

$$u = 1 + (U - 1)\exp(-\xi\eta) \tag{6}$$

As an example, one of the present results concerning $-f''(0)$ is compared in Fig. 2 with ones obtained from the local similar solution and Eq. (6) for $U = 2$ which corresponds to the shock Mach number 1.58 for $\gamma = 1.4$, where the results are truncated at $n = 4$ terms. It is seen from Fig. 2 that the local similar solution is effective just behind the shock wave, $\xi \ll 1$ and the present result approaches to the asymptotic suction profile for moderate ξ.

Though the present expansion method will not be applicable to far behind the shock wave, this method will sufficiently clarify

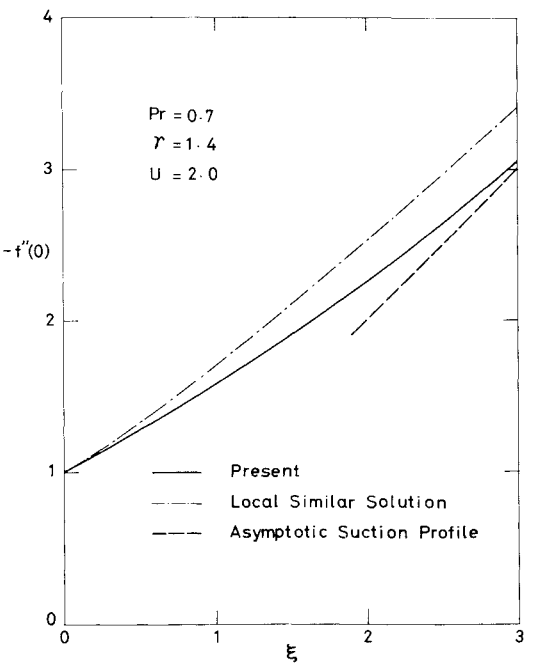

Fig. 2 Velocity gradients at the wall.

various aspects of the boundary layers developing behind the shock wave propagating along the perforated walls, because the important information we should have for the next research program comes mainly from the first parts of the boundary layer.

References

[1] Szumowski, A. P., "Attenuation of a Shock Wave along a Perforated Tube," *Shock Tube Research*, Chapman and Hall, London, 1971, pp. 14/1–14/10.

[2] Wu, J. H. T. and Ostrowski, P. P., "Shock Attenuation in a Perforated Duct," *Shock Tube Research*, Chapman and Hall, London, 1971, pp. 15/1–15/14.

[3] Honda, M., Takayama, K., and Onodera, O., "Studies on the Motion of Shock Waves Propagating along Perforated Ducts," *Report Institute High Speed Mechanics, Tohoku Univ.*, Vol. 30, No. 272, 1974.

[4] Mirels, H., "Boundary Layer Behind Shock or Thin Expansion Wave Moving into Stationary Fluid," TN 3712, 1956, NACA.

[5] Dorrance, W. H., *Viscous Hypersonic Flow*, McGraw-Hill, New York, 1962, pp. 26–32.

Axial Flow Measurements in Trailing Vortices

D. L. CIFFONE* AND K. L. ORLOFF†

NASA Ames Research Center, Moffett Field, Calif.

A SCANNING laser Doppler velocimeter[1–3] was used to measure the axial velocity defect in the cores of trailing vortices behind a lifting airfoil of rectangular planform. Data were obtained at several different angles of attack and downstream distances ranging from 30 to 10^3 chord lengths. The experiment was performed at the Univ. of California's water tow-tank facility at Richmond, Calif. The tank is 61 m long, 2.44 m wide, and 1.7 m deep. The test Reynolds number based on the wing chord was nominally 2.43×10^5. The wing used has an NACA 0015 airfoil section, an aspect ratio of 5.33, and a span of 0.61 m.

The existence of axial flow in the cores of lift-generated trailing vortices has been established experimentally,[2–8] with both defects and enhancements of the axial velocity being reported. With the exception of the water tank hydrogen bubble measurements of Ref. 7 and limited flight-test data, the experiments have been restricted to near field vortex characteristics. The present test was designed to obtain continuous data from the near field into the far field while removing uncertainties associated with the interpretation of data obtained by the hydrogen bubble technique. A detailed description of the present test procedure and data analysis is given in Ref. 8.

Batchelor[9] deduced the way in which the gradual slowing down of the rotary motion of the vortex by viscous action leads to an increased pressure at the core axis, resulting in an axial deceleration of the core fluid. He presents these effects explicitly in a similarity solution that is valid very far downstream. Brown,[10] using a modified Betz[11] calculation to describe the vortex flowfield, shows that the incremental axial velocity can be either forward or rearward, depending on the lift and profile drag coefficients of the wing. However, in contrast to Batchelor's work, Brown's results are expected to be valid only at relatively short distances behind the airfoil where the spiraling vortex is well rolled-up, but before the vorticity has been greatly spread and reduced in intensity by turbulent diffusion.

Moore and Saffman[12] consider the structure of a laminar trailing vortex behind a lifting wing and introduce viscosity to remove core centerline singularities, allowing the structure of the viscous core to be obtained. The pressure in the viscous core is then determined and used to calculate the axial velocities produced by streamwise pressure gradients. It is shown that the axial velocity can have a perturbation either away from or toward the wing, depending on the distribution of tip loading on the wing. The axial flow deficit in the core due to the presence of a boundary layer on the wing is also taken into account. For an isolated vortex from the tip of a rectangular planform wing with elliptic tip loading, the following approximate relationship (slightly modified from Ref. 12) is derived for the axial velocity at the core centerline V_x, normalized by the freestream velocity U_∞

$$\frac{V_x}{U_\infty} = (1 + 8.57 \times 10^{-5} \alpha^2 Re_c^{1/2}) \frac{0.28}{(x/c)^{1/2}} \tag{1}$$

where α is the angle of attack (in deg), Re_c is the Reynolds number based on a wing chord, and x/c is the downstream distance (in chord lengths). The derivation of Eq. (1) utilizes the approximation that $V_x \ll U_\infty$.

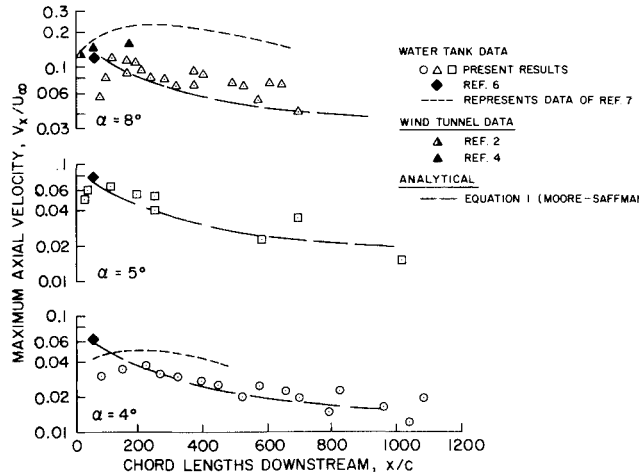

Fig. 1 Variation of maximum axial velocity with downstream distance; comparison of measurements with the laminar prediction of Moore and Saffman.[12]

Figure 1 compares the measured values of V_x/U_∞ with those predicted by Eq. (1). The agreement is remarkably good over the entire range of downstream distances, which supports the credibility of calculating axial velocities using the results of Moore and Saffman. Shown for comparison are the water tank data of Refs. 6 and 7 and the wind-tunnel data of Refs. 2 and 4. Agreement between the laminar prediction and the data improves as the angle of attack (α) decreases. This result is believed to be a consequence of the approximation that $V_x \ll U_\infty$ in the analysis.

References

[1] Grant, G. R. and Orloff, K. L., "A Two-Color, Dual Beam Backscatter Laser Doppler Velocimeter," TM X-62,254, 1973, NASA.

[2] Orloff, K. L. and Grant, G. R., "The Application of Laser Doppler Velocimetry to Trailing Vortex Definition and Alleviation," TM X-62,243, 1973, NASA.

[3] Ciffone, D. L., Orloff, K. L., and Grant, G. R., "Laser Doppler Velocimeter Investigation of Trailing Vortices Behind a Semi-Span Swept Wing in a Landing Configuration," TM X-62,294, 1973, NASA.

[4] Chigier, N. A. and Corsiglia, V. R., "Wind-Tunnel Studies of Wing Wake Turbulence," *Journal of Aircraft*, Vol. 9, No. 12, Dec. 1972, pp. 820–825.

[5] Logan, A. H., "Vortex Velocity Distributions at Large Downstream Distances," *Journal of Aircraft*, Vol. 8, No. 11, Nov. 1971, pp. 930–932.

[6] Olsen, J. H., "Results of Trailing Vortex Studies In a Towing Tank," in *Aircraft Wake Turbulence and Its Detection*, edited by J. H. Olsen, A. Goldberg, and M. Rogers, Plenum, New York, 1971, p. 455.

[7] Lezius, D. K., "Study of the Far Wake Vortex Field Generated by a Rectangular Airfoil in a Water Tank," TM X-62,274, 1973, NASA.

[8] Orloff, K. L., Ciffone, D. L., and Lorincz, D., "Airfoil Wake Vortex Characteristics in the Far Field," TM X-62,318, 1973, NASA.

[9] Batchelor, G. K., "Axial Flow in Trailing Line Vortices," *Journal of Fluid Mechanics*, Vol. 20, 1964, pp. 645–658.

Received January 21, 1974.

Index category: Jets, Wakes, and Viscid-Inviscid Flow Interactions.

* Research Scientist.

† Research Scientist. Associate Member AIAA.